JOURNAL OF AIRCRAFT
Vol. 40, No. 6, November–December 2003

Experimental Frossling Numbers for Ice-Roughened NACA 0012 Airfoils

Nihad Dukhan*
University of Puerto Rico at Mayaguez, Mayaguez, Puerto Rico 00681
Kenneth J. De Witt† and K. C. Masiulaniec‡
The University of Toledo, Toledo, Ohio 43606
and
G. James Van Fossen, Jr.§
NASA John H. Glenn Research Center at Lewis Field, Cleveland, Ohio 44135

Experimental Frossling numbers are presented for two aluminum castings of ice-roughened NACA 0012 airfoil surfaces at 0-deg angle of attack for chord Reynolds number ranging from 4.00×10^5 to 1.54×10^6. The castings were meticulously obtained from actual ice accretions representing mildly rough glaze and rough glaze ice with horns. A modified investment casting technique was used to capture all of the surface roughness details. The rough glaze ice with horns produced higher heat-transfer rates than those for the mildly rough glaze ice, especially at the horns. Immediately downstream of the horns, stagnation air gaps resulted and caused lower heat-transfer coefficients. For both types of ice, higher Reynolds numbers in general produced higher heat-transfer coefficients. For the same chord Reynolds number and at the same position on the airfoil, the Frossling numbers were generally higher than those for the smooth case and those for the hemispherical roughness elements of previous studies. A maximum increase of approximately 306% over the smooth case and 192% over the dense hemispherical roughness case was recorded at one rough glaze ice horn. This work provides some directly measured values of the Frossling number needed to improve the prediction of some icing codes. Such icing codes help in the effective design of some deicing systems of aircraft.

Nomenclature

A	=	area of test tile
a_1-a_5	=	constants for Eq. (5)
c	=	chord
c_p	=	specific heat of air at constant pressure
c_1, c_2	=	constants for Eq. (6)
D	=	average diameter of a roughness element
Fr	=	$Nu/\sqrt{(Re)}$, Frossling number based on chord
H	=	average ice roughness element height
h	=	heat-transfer coefficient
k	=	thermal conductivity of air
Nu	=	hc/k, Nusselt number based on chord
Q_{btm}	=	heat loss by conduction through bottom guard tile
Q_{elec}	=	electric power input
Q_{gap}	=	heat loss by conduction through epoxy gap between test tiles
Q_{rad}	=	heat loss by radiation
Re	=	uc/ν, Reynolds number based on chord
S	=	average spacing of ice roughness elements
s	=	distance from the leading edge
T	=	average temperature of test tile
T_∞	=	ambient temperature in wind tunnel
U	=	axial freestream velocity in the icing wind tunnel for ice accretion
u	=	mean axial velocity of airflow for heat-transfer measurements
ν	=	kinematic viscosity of air

Received 22 January 2003; revision received 17 May 2003; accepted for publication 21 May 2003.

*Visiting Professor, Mechanical Engineering Department, P.O. Box 9045.
†Professor, Chemical Engineering Department, 2801 W. Bancroft.
‡Associate Professor, Mechanical Industrial and Manufacturing Engineering Department, 2801 W. Bancroft.
§Senior Research Scientist, 21000 Brookpark Road.

Introduction

THE severe degradations in aerodynamic performance associated with accreted ice on airfoil surfaces are well known. Large and rapid increases in drag of 300 to 400% were recorded by Gray and Von Glahn,[1] Gray,[2] and Mullins et al.,[3] and a reduction of 40 to 60% in the maximum lift coefficient was recorded by Smith et al.[4] The magnitude of these penalties was a function of the shape and the size of the ice accretion, which were complex functions of operating and icing conditions, that is, air speed and temperature, angle of attack, liquid water content, droplet size, and icing time.[1] These penalties were more severe in the laminar flow case.[4] Furthermore, the subsequent shedding of the ice, natural or induced, causes damage upon striking sections of an airframe because of the high velocities involved. The impact force could reach values as high as 9000 N, as reported by Singh et al.[5] References 6–10 are more recent studies regarding the negative effects of icing on the performance of airfoils.

Ice accretions are generally classified as rime or glaze ice. In general, colder temperature and lower liquid water contents produce rime ice accretions. The icing process in this case is quick such that air pockets are trapped in the ice formation, which gives this type of ice a somewhat white color. Warmer temperatures and higher liquid water contents, on the other hand, generally produce glaze accretions. In this case, the icing process is not as fast, and the resulting ice is clear.[11]

To utilize deicing or anti-icing systems, most computational schemes that predict ice accretions rely on empirical relationships for the convective heat-transfer rates from the surface of the accreted ice, with some corrections to account for the effect of roughness. Predictions of the ice growth rates and the resulting shapes, using these codes, are extremely sensitive to the values used for the heat-transfer coefficient. This is so because the convective heat transfer is a prominent mechanism in any thermal analysis of the icing process.

Ice accretion predictions by NASA's LEWICE, for example, called for refinement or replacement of the current empirical relationships (especially for glaze ice) with new relationships that give more representative or physically correct values of the convective heat-transfer coefficient.[12]

Prior to 1984, no data for heat-transfer coefficients from ice shapes existed in the open literature. Van Fossen et al.[13] presented experimental values of the heat-transfer coefficient from polyurethane foam castings of simulated ice accretion shapes on a long cylinder. For the 2-min-glaze ice the heat transfer remained the same in the stagnation region as for the smooth model, but boundary-layer transition caused by roughness caused heat transfer to nearly triple at 45.0 deg from the stagnation point. For the 5-min glaze ice accumulation, roughness caused heat transfer to increase with distance away from the stagnation point. The maximum increase occurred at 46.3 deg from the stagnation point and was nearly double that of the smooth surface case.

The quantitative work describing the size and the distribution of the roughness associated with ice formation on airfoils is also scarce. Shin[14] used an optical imaging technique to investigate the glaze ice accretion phenomenon on a NACA 0012 airfoil. The airfoil had a 0.53-m (21-in.) chord and a 1.83-m (6-ft) span. Airspeeds ranged from 67.1 to 111.8 m/s; air temperatures from -3.9 to -1.1°C; and liquid water content from 0.5 to 1.2 g/m^3.

Poinsatte et al.[15] presented experimental heat-transfer data from a smooth NACA 0012 airfoil for chord Reynolds numbers in the range 1.24×10^6 to 2.50×10^6 and various angles of attack up to 4 deg. The airfoil had a chord length of 0.533 m (21 in.) and a span length of 1.8 m (6 ft). For the 0-deg case the Nusselt number data correlated well with the square root of the Reynolds number. The Frossling number was greatest at the stagnation point, and it trailed off smoothly to an average value of about 1.0 at the dimensionless distance s/c of 0.083, with an unexplained jump at $s/c = 0.048$.

In a different study Poinsatte et al.[16] presented experimental heat-transfer data for roughened NACA 0012 airfoils. Artificial roughness was obtained by attaching 2-mm-diam hemispheres arranged in four different patterns: leading-edge roughness, sparse roughness, and two different dense roughness arrangements. The hemispheres were spaced 10 or 20 mm apart spanwise. The leading-edge roughness case was obtained by attaching four hemispheres spaced 20 mm apart to the stagnation line. The sparse case was obtained by attaching three or four hemispheres, in an alternating fashion on every third tile, also spaced 20 mm apart. The two dense cases had seven roughness elements on the geometrical stagnation line, six between the first and the second tile on the high-pressure side of the airfoil, followed by seven on the seventh tile, all spaced 10 mm apart. For dense 1 case the density then decreased. Only four elements were attached to the tenth tile, and three to the thirteenth tile, spaced 20 mm apart. Unlike the dense 1 case, the other dense case, dense 2, did not have a decrease in the roughness density. The leading-edge roughness had little effect: it locally increased the heat transfer at the leading edge by about 10% over the smooth airfoil case but did not affect the heat transfer downstream. For the sparse roughness there was an increase in heat transfer at the leading edge followed by increases at, and immediately downstream of, each roughness row. For the dense 1 and the dense 2 roughness patterns the roughness, in general, drastically increased the heat-transfer rates. Increasing the density of the roughness elements from the sparse to the dense patterns caused yet a higher increase in heat transfer ranging from 32 to 54%. Increasing the angle of attack also caused heat transfer to increase over the 0-deg case, and the angle-of-attack dependence was much more prominent in the dense roughness cases.

Pais et al.[17] used wind-tunnel measurements to obtain the local-convective heat-transfer coefficients for 0- (smooth) and 5-min simulated glaze-like ice models on a NACA 0012 airfoil. For the smooth model data were collected at the angles of attack 0, 2, 4, 6, and 8 deg; and for the 5-min glaze model data were collected at 4 deg only. The chord Reynolds number range was 7×10^5 to 2×10^6. For the smooth model at 2, 4, 6, and 8 deg, the relative increase of the Nusselt number on the suction surface with respect to the pressure surface was 21, 36, 58, and 72%, respectively. The results for the 5-min model showed that the maximum Nusselt number occurred at the tip of the glaze horn where it was 51% higher than on the rest of the surface and 25% higher than the same surface location without ice accretion. Results also pointed to stagnation and separated flow regions after the horns.

Although very valuable, previous studies are lacking in one or both of the following aspects: 1) testing and studying the heat transfer from actual ice shape roughness and 2) combining the effect of actual ice roughness with the curvature of airfoils. This study overcomes these two issues for one type of airfoil only. It investigates the effect of ice roughness on two models of ice-roughened NACA 0012 airfoils. Thus, it combines the effect of ice roughness with the effect of acceleration caused by the actual curvature of the airfoils. A NACA 0012 airfoil was chosen because of its symmetric profile, which is commonly used in helicopter rotors. Such aircraft fly at lower altitudes and thus are more susceptible to ice accretion.

The present effort is the third in a series of fundamental studies investigating the roughness problem that is associated with ice accretion. The first study[18] isolated the effect of different types of ice roughness (different ice accretions under different icing conditions) on flat plates and compared that to the smooth plate case and to other types of uniform roughness, that is, hemispheres and truncated cones. The second[19] combined the effect of the ice roughness with acceleration induced by the inclination of the flat plate models. The current study investigates the heat transfer from ice-roughened NACA 0012 airfoils. It produces direct, accurate, and well-posed experimental data sets of the convective heat-transfer coefficient from the airfoil ice-roughened surfaces, which are important for their intrinsic value and are also essential for numerical codes that simulate ice accretion. Additionally, a good knowledge of the range of heat losses that can be expected with different types of ice accretions provides some of the information required to effectively size and design different types of in-flight deicing systems.

Investment Casting

Two different ice accretions were obtained on two NACA 0012 airfoils with a chord length of 0.53 m (21 in.) in the Icing Research Tunnel at the NASA John H. Glenn Research Center at Lewis Field (LeRC), Cleveland, Ohio. Table 1 lists the icing tunnel conditions for the two ice accretion cases.

Because of the similarity of the icing tunnel conditions, the characterization of the accreted ice was estimated based on the measurements and the reported parameters of Shin.[14] The estimated parameters of the two ice roughness cases of this study are shown in Table 2. This characterization does not include the horns in the case of the fully rough glaze ice.

Aluminum castings of these ice accretions were then meticulously obtained, with all of the microscopic details intact, using a modified

Table 2 Estimated roughness parameters based on Shin[14]

Ice character	H, mm	S, mm	D, mm
Mildly rough glaze	0.62	1.33	1.15
Rough glaze with horns	0.55[a]	1.18[a]	1.05[a]

[a]Estimated based on Shin's[14] study for the same icing conditions but 6-min accretion time.

Table 1 Tunnel icing conditions

Run	T, °C	U, m/s	LWC, g/m^3	MVD, μm	Spray time, s	Ice character
1	-2.22	67.05	0.5	20	180	Mildly rough glaze
2	-2.22	67.05	0.5	20	450	Rough glaze with horns

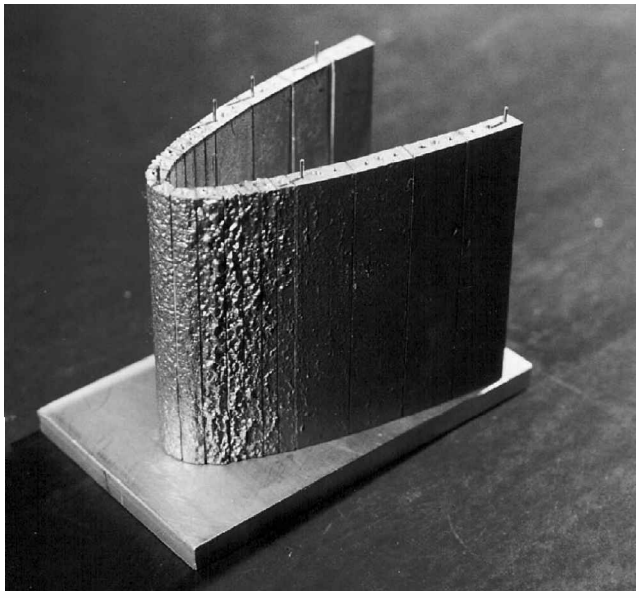

Fig. 1 Photograph of the aluminum casting of mildly rough glaze ice accretion on a NACA 0012 airfoil.

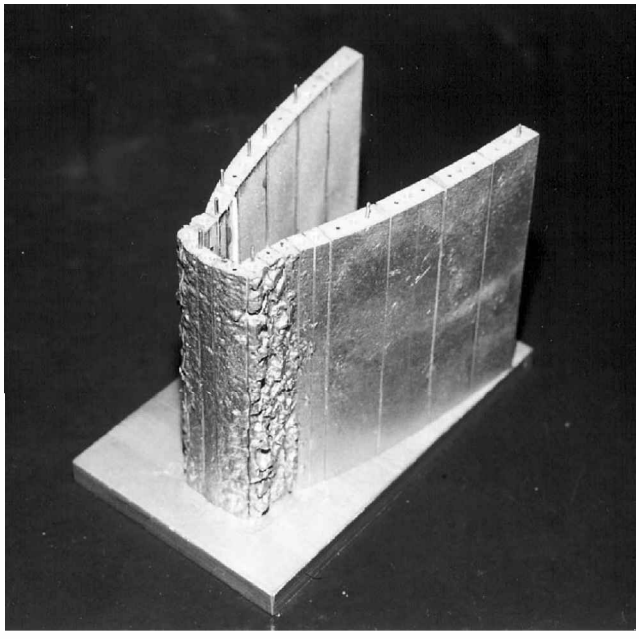

Fig. 2 Photograph of the aluminum casting of rough glaze ice accretion with horns on a NACA 0012 airfoil.

investment casting technique. For more details about the casting technique, see Refs. 18 and 20. The investment casting process was used because it is most flexible with respect to attainable intricacy and precision (average tolerance $\pm 9.0 \times 10^{-5}$ m) (Ref. 21).

Two refractory molds were first obtained. Each mold was placed in a furnace and was fired at a temperature of 649 to 760°C (1200 to 1400°F) for at least two hours. After firing, each mold was allowed to cool to the desired casting temperature of approximately 427°C (800°F). Molten 356-aluminum at a slightly higher temperature was then poured into each of the ceramic molds capturing as much of the microscopic surface detail as possible. After complete solidification of the aluminum, the ceramic molds were broken off and separated from the aluminum castings. Figures 1 and 2 show the two aluminum castings of the ice-roughened airfoils representing the mildly rough glaze and the rough glaze ice with horns, respectively.

Model Construction

Two experimental models were constructed from the two aluminum castings. Each model was in essence a large composite of many heat-flux gauges and guard heaters. The test bed consisted of a row of 21 test tiles each being approximately 0.066 m (2.6 in.) in span. The width of each tile in the flow direction varied depending on the character of the ice accretion at the particular tile. Small-width tiles were used when the density of the ice was high, or where there was a variation in the character to be captured by the test. More tiles were used around the leading edge because ice accretion is primarily a leading-edge phenomenon. Table 3 lists the width of each tile for the two roughness models, as well as the numbering scheme in relation to the dimensionless surface distance s/c for each tile. Biot number calculations showed that such dimensions were suitable for the assumption of a constant locally averaged temperature for each tile.

The test tiles were cut using an electric discharge machine to minimize the metal loss caused by cutting and thus preserving the actual roughness elements' integrities, as can be seen in Figs. 1 and 2. Figures 3 and 4 are cross-sectional plots of the airfoils for the mildly rough and the rough glaze ice with horns cases, respectively. These two-dimensional figures can be traced and used as a geometrical input to some of the icing codes as described in Ref. 22. To provide heat, each test tile was instrumented with a standard thermofoil heater. The heaters covered most of the bottom surface area of the tiles in order to provide uniformly distributed heat input.

On one side of each of the test tiles and at approximately 0.006 m below the outer surface, a 0.002-m diam, 0.033-m deep hole was

Table 3 Widths of test tiles and numbering scheme

	Mildly rough glaze		Rough glaze with horns	
Tile no.	Width, mm	Surface distance, s/c	Width, mm	Surface distance, s/c
1	21	——	22	——
2	19	−0.116	20	−0.122
3	19	−0.091	21	−0.094
4	18	−0.065	21	−0.066
5	5	−0.048	5	−0.049
6	5	−0.041	5	−0.042
7	5	−0.034	4	−0.035
8	5	−0.025	6	−0.027
9	8	−0.019	8	−0.018
10	7	−0.010	11	−0.010
11	11	0.000	6	0.000
12	5	0.010	9	0.008
13	8	0.018	7	0.017
14	5	0.026	8	0.026
15	6	0.033	5	0.033
16	5	0.040	5	0.039
17	5	0.047	5	0.047
18	19	0.063	20	0.061
19	19	0.089	21	0.089
20	20	0.115	21	0.117
21	20	——	21	——

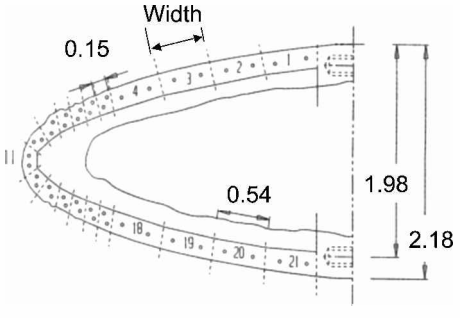

Fig. 3 Contour drawing of the mildly rough glaze ice accretion on a NACA 0012 airfoil with test tiles numbering scheme (dimensions in inches).

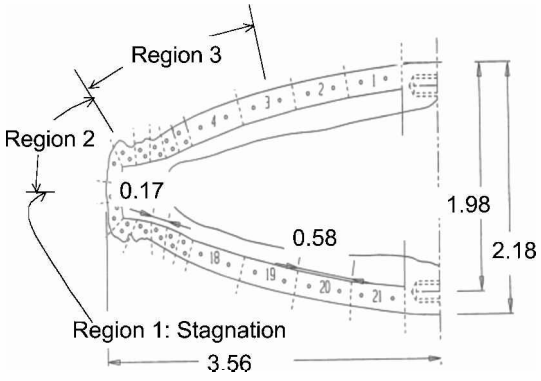

Fig. 4 Contour drawing of the rough glaze ice accretion with horns on a NACA 0012 airfoil with test tiles numbering scheme (dimensions in inches).

drilled. Each hole housed the bead of a thin Chromel-Alumel thermocouple to measure the average temperature of the tile.

The test tiles were glued together using epoxy and plastic spacing shims to ensure a uniform gap between all of the tiles and to thermally insulate the tiles from each other. Three guard heaters were placed in the inside of the airfoil model to prevent conduction to the inside of the model. Each guard heater was supplied with enough heat such that it was maintained at the same temperature as the outer surface of the airfoil. The three guard heaters also provided the primary structural support for the model.

Wind-Tunnel Testing and Data Reduction

The heat-transfer experiments were carried out in the wind tunnel described in detail by Van Fossen et al.[13] The LeRC's ESCORT data-acquisition system was utilized for the data collection and reduction. Heat-transfer data for each of the two rough models were collected for freestream velocities of 11.8, 21.2, 33.7, and 45.0 m/s; and with a surface-to-free-stream temperature difference of approximately 15.3 and 18.5°C for the mildly rough glaze and the rough glaze with horns models, respectively. The angle of attack was 0 deg.

The desired flow rates in the tunnel were established and were allowed to reach steady state before data were taken. The freestream turbulence level was under 0.5% throughout the experiment. A control circuit automatically adjusted the power input to each of the test tiles so that the average temperature of each tile was within ±0.25°C of the set value. To eliminate conductive losses, the guard tiles were maintained at the same temperature. The power input to each tile (energy flux), which compensated for the heat loss by convection from the outside surface, was recorded and, along with the surface and tunnel temperatures, provided the needed information for the heat-transfer coefficient calculations.

Reduction of the raw data was performed by a computer code that was developed, used, and then was modified by Van Fossen et al.[13] The locally averaged heat-transfer coefficient for each gauge was determined by subtracting the heat losses from the measured electrical power input to each of the individual tiles:

$$h = \frac{Q_{\text{elec}} - Q_{\text{rad}} - Q_{\text{gap}} - Q_{\text{btm}}}{A(T - T_\infty)} \tag{1}$$

The radiation loss Q_{rad} was on the order of 0.2%, and it was calculated assuming gray-body radiation to black surroundings and an emissivity of 0.05 for the aluminum tiles. The loss caused by the epoxy gap Q_{gap} between the test tiles was about 2%, and it was obtained from an exact solution for two-dimensional conduction in a rectangular slab.[13] At high heat fluxes a significant temperature gradient developed between the heater and the imbedded thermocouple. This made it impossible to adjust the bottom guard temperature to exactly match the heater temperature, thus allowing a small amount of heat Q_{btm} to leak to the bottom of the guard tiles which was accounted for by assuming one-dimensional heat conduction. This gap's loss was also about 2% of the total heat flow.

The measurement uncertainty associated with the results of this study was calculated using the method of Kline and McClintock.[23] Using Eq. (1), the uncertainty in the heat-transfer coefficient was calculated by

$$\frac{\mathrm{d}h}{h} = \left[\left(\frac{\mathrm{d}Q_{\text{elec}}}{Q_{\text{conv}}}\right)^2 + \left(\frac{\mathrm{d}Q_{\text{rad}}}{Q_{\text{conv}}}\right)^2 + \left(\frac{\mathrm{d}Q_{\text{gap}}}{Q_{\text{conv}}}\right)^2 + \left(\frac{\mathrm{d}Q_{\text{btm}}}{Q_{\text{conv}}}\right)^2 + \left(\frac{\mathrm{d}A}{A}\right)^2 + \left(\frac{\mathrm{d}T}{T - T_\infty}\right)^2 + \left(\frac{\mathrm{d}T_\infty}{T - T_\infty}\right)^2\right]^{\frac{1}{2}} \tag{2}$$

The Frossling number was calculated using the heat-transfer coefficient by

$$Fr = NuRe^{-0.5} = (hc/k)(uc/\nu)^{-0.5} \tag{3}$$

The uncertainty in the Frossling number was calculated in a similar manner using Eq. (3). The resulting uncertainty in the Frossiling number was 9.7%.

Experimental Results

The heat-transfer results will be presented using the Frossling number, which is defined in Eq. (3). Like the Stanton number, the Frossling number is a dimensionless number occasionally used to present convection heat-transfer data. Stanton number, however, accounts for the changes in the transport properties because it includes Prandtl number. Frossling number was a better choice for this study because the Prandtl number was essentially constant as a result of the small temperature variations. From Eq. (3) and at a given Reynolds number, the Frossling-number variation represents the variation in the heat-transfer coefficient.

In the following discussion the numbering scheme of Table 3 should be used to establish the relationship between any tile number and the dimensionless surface distance, s/c, from the leading edge to the center of the tile.

Figure 5 is a composite plot of the Frossling number versus the dimensionless surface distance for the mildly rough glaze ice at the four different Reynolds numbers of this study. The solid curve represents the case for the smooth airfoil at the highest Re of 1.52×10^6 adapted from Poinsatte et al.[15] As expected, the surface roughness due to this type of ice produced higher heat-transfer rates than those for the smooth case. Shin[14] stated that for the 2- and 3-min glaze ice, the roughness height is well above the boundary layer thickness and the critical roughness height, thus transition to turbulence occurs. This explains the increase in heat-transfer and the immediate departure from the smooth airfoil case.

At the highest Re, the mildly rough glaze ice produced a maximum increase of about 188.6% over the smooth case ($Fr = 10.1$ approximately). The location of this increase is at tile no. 13 according to

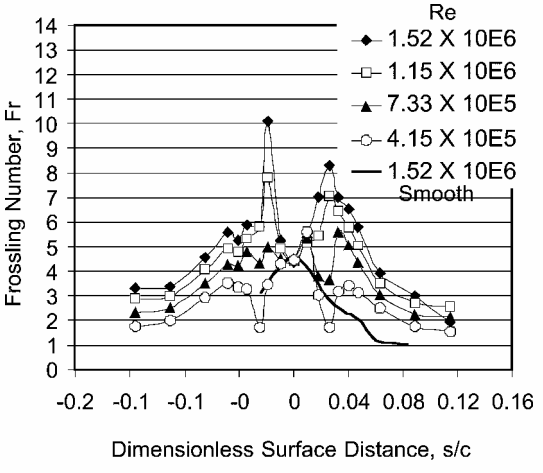

Fig. 5 Heat transfer from mildly rough glaze ice accretion on a NACA 0012 airfoil at different Reynolds numbers (uncertainty 9.7%).

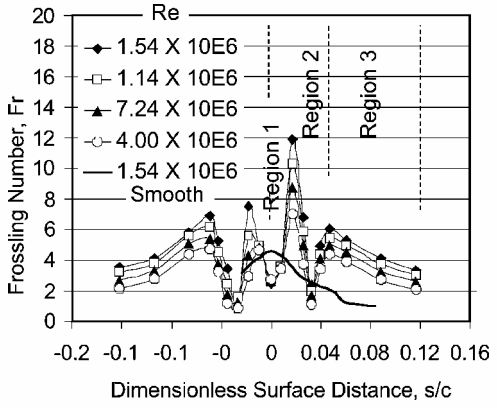

Fig. 6 Heat transfer from rough glaze ice with horns accretion on a NACA 0012 airfoil at different Reynolds numbers (uncertainty 9.7%).

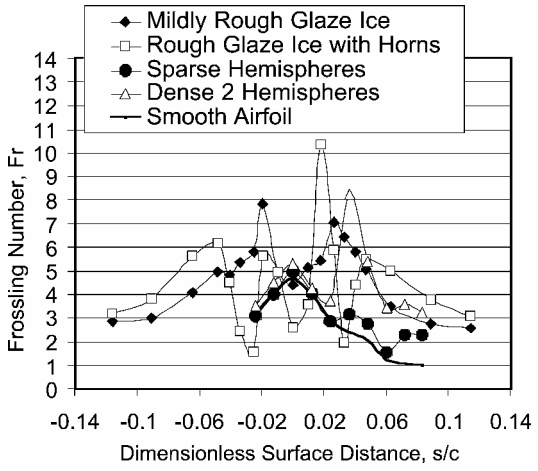

Fig. 7 Heat-transfer comparison between ice and hemispherical roughness for a NACA 0012 airfoil at $Re = 1.15 \times 10^6$ (uncertainty 9.7%).

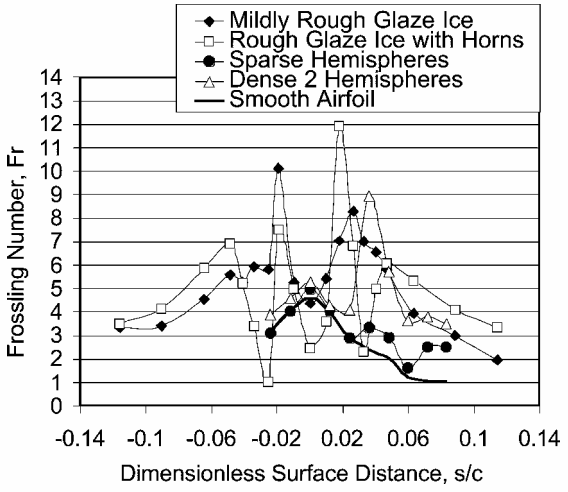

Fig. 8 Heat-transfer comparison between ice and hemispherical roughness for a NACA 0012 airfoil at $Re = 1.52 \times 10^6$ (uncertainty 9.7%).

the numbering scheme of Fig. 3. Inspection of this figure reveals that there is a somewhat sudden increase in the roughness height for that tile. Actually, because of this the Frossling number has a local maximum at this tile for all of the Reynolds-number cases except for the lowest Reynolds number of 4.18×10^5. The same argument can be made about tile no. 8 on the top surface of the airfoil for the Reynolds-number cases of 1.52×10^6 and 1.15×10^6. For $Re = 7.33 \times 10^5$ the maximum Frossling number occurs at tile no. 7; and for $Re = 4.15 \times 10^5$ the maximum occurs at tile no. 6. The relatively minor shift of the location of the maximum heat-transfer rate is attributed to the flowfield behavior at the sudden roughness height increase around those tiles. The local minima at tile no. 8 on the top surface of the airfoil and at tile no. 14 on the bottom surface for $Re = 4.15 \times 10^5$ and 7.33×10^5 are most likely caused by flow separation of the boundary layer after the high roughness elements close to these tiles. Pais et al.[17] pointed to stagnation and separated flow regions after the horns. Away from the rough region, which is close to the leading edge, that is, for a dimensionless surface distance $s/c > 0.04$, the Frossling number is well behaved and increases with increasing Reynolds number.

Figure 6 is a composite plot of the Frossling numbers for the four Reynolds-number cases for the rough glaze ice with horns. The horns are seen to drastically dictate the Frossling-number behavior. The spike at tile no. 9 has a maximum of $Fr = 12.0$ approximately and is caused by the horn on the top surface of the airfoil, which can be seen in Fig. 4. A similar behavior is seen for tile no. 13 on the bottom surface, where the Frossling number sets at about 7.5. The Frossling number sets below the smooth case at tile no. 7 on the top surface and tile no. 14 on the bottom surface. This is caused by flow separation, reversal, and pockets of stagnant air immediately following the relatively high horns as indicated by Pais et al.[17] The heat transfer from the leading edge for this roughness model is lower than that for the smooth case. This is caused by the very drastic difference in the flowfield dictated by the presence of the horns, which produces a significantly different geometry over which the flow has to travel. The Frossling number increases with increasing Reynolds number and is well behaved away from the leading edge, that is, for $s/c > 0.05$, that is, tiles 5, 4, 3, and 2.

Comparison to Hemispherical Roughness

Comparisons were made with Poinsatte et al.[16] in order to contrast the heat transfer in the random roughness element case (ice roughness) with that for a well-defined roughness element case, that is, the hemispheres. In particular, Poinsatte et al.'s[16] sparse and dense 2 cases were chosen at Reynolds numbers of 1.15×10^6 and 1.52×10^6. This was decided because of the relatively small difference in the values of the Reynolds numbers of their work and of this study. Their leading-edge roughness had little effect: it locally increased the heat transfer at the leading edge by about 10% over the smooth airfoil case and did not affect the heat transfer downstream. Their dense 1 case was not included in the comparison plots because it would clutter them hopelessly.

Figure 7 provides a comparison between the two ice roughness cases of this study and Poinsatte et al.'s[16] sparse and dense 2 cases. The smooth airfoil case of Poinsatte et al.[15] is included for reference. As shown in Fig. 8, at the tip of the horn of the rough glaze ice (tile no. 9) the Frossling number is approximately 27% higher than the maximum for the dense 2 case, which occurs at a dimensionless distance s/c of about 0.035. For the sparse case this increase is about 110%, with the maximum Frossling number for the sparse case occurring at the leading edge. Poinsatte et al.'s[16] Frossling-number data for the dense 2 case and for the sparse roughness case generally lie below both of the ice roughness cases of this study. The exceptions are the peak for the dense 2 case and the minimum for tile no. 7 following the rough glaze horn; also the last two data points for $s/c > 0.06$ for the dense 2 case. The latter is because at these locations there was hemispherical roughness attached in the dense 2 case of Poinsatte et al.[16] However, for the current ice roughness study there is very small ice roughness at this relatively far distance from the leading edge, that is, most of the ice roughness is concentrated at the leading edge. It is clear that the presence of the horns in the ice roughness case is a more severe disturbance to the flowfield when compared to the hemispherical roughness. This is because the ice horns had a height of approximately 5 mm compared to the hemispherical roughness, which had a height of only 1 mm. The random roughness element shapes in the case of ice also enhance the heat transfer by providing more turbulence compared to the smooth symmetrical shape of a

hemisphere. This roughness element shape effect was also observed by Dukhan et al.[18] and Hosni et al.[24] The roughness spacing is less in the random roughness cases, which increases the heat transfer. This phenomenon was noted in the previous studies of Dukhan et al.[18] and Hosni et al.[25] The spacing for the mildly rough glaze and for the rough glaze ice with horns are 1.15 and 1.05 mm, as shown in Table 2, whereas they are 20.00 and 10.00 mm for the sparse and the dense 2 cases, respectively. The heat transfer at the stagnation point is higher than in the case of the hemispherical roughness. This is so because there were hemispherical roughness elements attached at the leading edge for all of Poinsatte et al.[16] roughness cases.

Figure 8 compares the two ice roughness cases to those of the hemispherical roughness sparse and dense 2 cases of Poinsatte et al.[16] at the highest Reynolds number of this study $Re = 1.54 \times 10^6$. The smooth airfoil case of Poinsatte et al.[15] is again included for reference. Similar trends as those of Fig. 7 are observed. In Fig. 8 and at the tip of the horn of the rough glaze ice (tile no. 9), the Frossling number is approximately 31% higher than the maximum for the dense 2 case, which occurs at a dimensionless distance s/c of about 0.035. For the sparse case this increase is about 134%, with the maximum Frossling number for the sparse case occurring at the leading edge. These differences are a little higher for this higher Reynolds number compared to those for the lower Reynolds number of 1.15×10^6. This is probably caused by the effect of the roughness character on the boundary-layer development as the Reynolds number increases.

Heat-Transfer Polynomials

Inspection of Figs. 5 and 6 shows that the greatest heat transfer occurs at the top surface of the rough glaze ice with horns. It also shows that the behavior of the Frossling number is consistent along the chord for all Reynolds numbers in this case. This is caused by the fact that the heat transfer is dictated by the flowfield around the horns. In other words, the rough glaze with horns is a more deterministic surface. These observations cannot be made for the mildly rough glaze case, that is, there are significant differences in the curves for the two lower Reynolds numbers and the two higher Reynolds numbers. So attention is given to the top surface of the rough glaze ice with horns. From Fig. 6 it is clear that the two horns on the top and the bottom surfaces produce vastly different Frossling numbers. So there could be no single equation that can describe them both. Also, the heat-transfer rates are more severe for the top surface, so that an equation for that surface would represent the worst case.

Inspection of Fig. 6 along with an understanding of the fluid mechanic behavior at and immediately after the horns both reveal that there are three distinct heat-transfer regions. The first is at the stagnation point or the leading edge; the second from the leading edge to a surface distance of $s/c < 0.047$. The third region is from that location to the trailing edge of the airfoil, that is, $s/c \geq 0.047$. The second region includes the flow over and the heat transfer at the tip of the horn as well as immediately after the horn and up to where the flow, and thus the associated convective heat transfer, seems to "recover" from the effect of the horn. Heat-transfer equations (curve fits) were sought for the three regions.

Region 1: The Stagnation Point

The Frossling number at the stagnation point was a quadratic function of the Reynolds number as shown graphically in Fig. 9 and by Eq. (4).

$$Fr = -7.32 \times 10^{-14} Re^2 - 8.92 \times 10^{-8} Re + 2.81 \qquad (4)$$

Region 2: Around The Horn

For the second region, not including the stagnation point and the point $s/c = 0.047$, curve fits of the Frossling number as a function of the distance along the airfoil s/c, using a polynomial of degree four, are shown in Fig. 10. The general form of this polynomial is given by

$$Fr = a_1(s/c)^4 + a_2(s/c)^3 + a_3(s/c)^2 + a_4(s/c) + a_5 \qquad (5)$$

The constants a_1–a_5 , listed in Table 4, were determined from the curve fits.

Table 4 Constants for Eq. (5)

Re	a_1	a_2	a_3	a_4	a_5
1.54×10^6	2.00×10^7	1.00×10^6	-1.93×10^5	4942.3	−24.76
1.14×10^6	2.00×10^7	6.09×10^5	-1.46×10^5	3936.1	−19.24
7.24×10^5	3.00×10^7	-6.48×10^5	-8.27×10^4	2705.5	−12.85
4.00×10^5	3.00×10^7	-4.55×10^5	-6.73×10^4	2102.1	−9.13

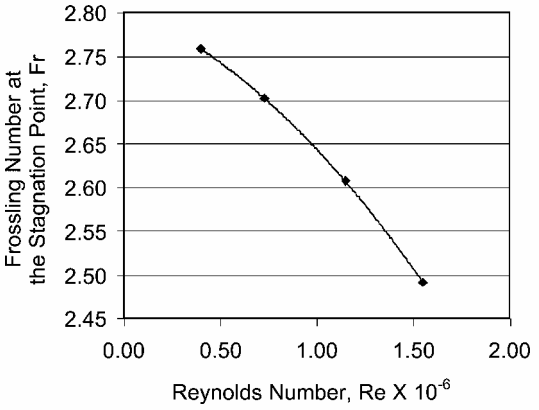

Fig. 9 Curve fit of the Frossling number in region 1: stagnation point.

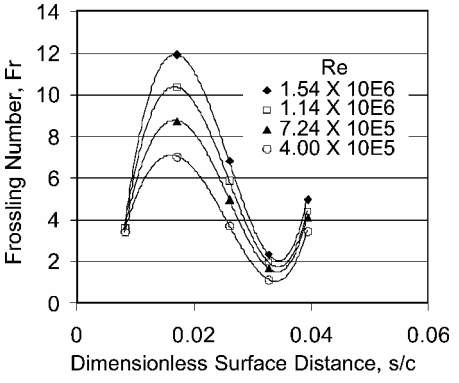

Fig. 10 Curve fit of the Frossling number in region 2: around the horn.

Region 3: After the Horn

For each location s/c in this region, the Frossling number was a linear function of the Reynolds number as shown in Fig. 11 and by Eq. (6).

$$Fr = c_1 Re + c_2 \qquad (6)$$

The constant c_1 was equal to 1.00×10^{-6} for all locations in this region. The constant c_2 on the other hand varied with the location according to Eq. (7) and is shown in Fig. 12.

$$c_2 = 11087(s/c)^3 - 2571.4(s/c)^2 + 154.14(s/c) + 1.17 \qquad (7)$$

Substituting for c_2 into Eq. (6), the following general equation for this region is obtained:

$$Fr(Re, s/c) = 1.00 \times 10^{-6} Re + 11087(s/c)^3 - 2571.4(s/c)^2 + 154.14(s/c) + 1.1739 \qquad (8)$$

Equation (8) can predict the Frossling numbers in this third region with good accuracy.

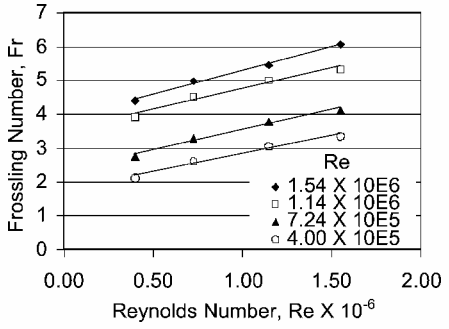

Fig. 11 Curve fits of the Frossling number in region 3: after the horn.

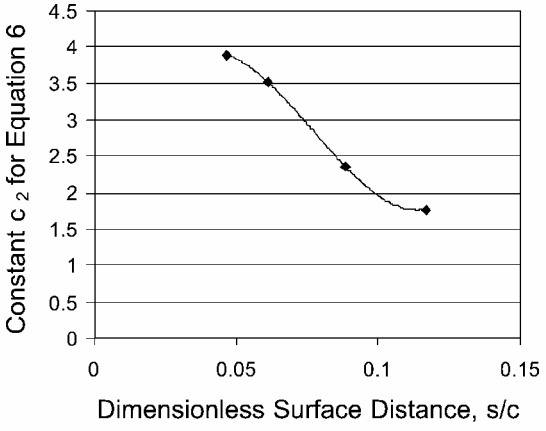

Fig. 12 Curve fit of the constant c_2 for correlation 6.

Conclusions

Frossling-number results were obtained for the rate of convective heat transfer from aluminum castings of ice-roughened surfaces. The castings were obtained from stochastically accreted ice on two NACA 0012 airfoils in the Icing Research Tunnel at the NASA John H. Glenn Research Center at Lewis Field, Cleveland, Ohio. Two basic types of ice accretions were considered: mildly rough glaze and rough glaze with horns. The two models were tested in a wind tunnel for freestream velocities of 11.8, 21.2, 33.7, and 45.0 m/s. The highest rate of heat transfer was recorded at the horns and reached values 306% higher that those obtained with a smooth model at the same location and for the same Reynolds number.

The Frossling numbers obtained in this study were generally higher than those obtained in heat-transfer roughness studies using hemispherical roughness elements. And the data showed transition very close to the leading edge.

Three distinct heat-transfer regions were identified and were related to the surface geometry and the resulting flowfield. Curve fits for the Frossling number in each region with the flow Reynolds number and/or the surface distance from the leading edge were obtained. This was done for the top surface of the rough glaze with horns only. These curve fits predict the Frossling numbers for that particular surface with very good accuracy.

The data obtained can be used in some numerical codes for predictions of accreted ice shapes.

Acknowledgment

The authors express their gratitude to the Icing and Cryogenics Technology Branch at the NASA John H. Glenn Research Center at Lewis Field, Cleveland, Ohio, for funding this effort under Grant NAG 3-72 and the Heat Transfer Branch for their help and allowing the use of their facilities, especially Jaiwon Shin, Mario Vargas, and David Anderson.

References

[1]Gray, V. H., and Von Glahn, U. H., "Aerodynamic Effect Caused by Icing of an Unswept NACA 65A004 Airfoil," NACA TN 4155, Feb. 1958.

[2]Gray, V. H., "Prediction of Aerodynamic Penalties Caused by Ice Formation on Various Airfoils," NASA TM D-2166, Feb. 1964.

[3]Mullins, B., Jr., Smith, D., and Korkan, K., "Effect of Icing on the Aerodynamics of a Flapped Airfoil," AIAA Paper 95-0448, Jan. 1995.

[4]Smith, D., Mullins, B., Jr., and Korkan, K., "Effect of Icing on the Aerodynamic Performance of a Series of Two Dimensional Airfoils at Low Reynolds Numbers," AIAA Paper 95-0453, Jan. 1995.

[5]Singh, S., Masiulaniec, K. C., De Witt, K. J., and Britton, R., "Measurements of the Impact Forces of Shed Ice Striking a Surface," AIAA Paper 94-0713, Jan. 1994.

[6]Calay, R. K., Holdø, A. E., Mayman, P., and Lun, I., "Experimental Simulation of Runback Ice," *Journal of Aircraft*, Vol. 34, No. 2, 1997, pp. 206–212.

[7]Lee, S., and Bragg, M. B, "Experimental Investigation of Simulated Large-Droplet Ice Shapes on Airfoil Aerodynamics," *Journal of Aircraft*, Vol. 36, No. 5, 1999, pp. 844–850.

[8]Chung, J., Reehorst, A., Choo, Y., Potapczuk, M., and Slater, J., "Navier–Stokes Analysis of Flowfield Characteristics of an Ice-Contaminated Aircraft Wing," *Journal of Aircraft*, Vol. 37, No. 6, 2000, pp. 947–959.

[9]Cuerno-Rejado, C., López-Martínez, G., Escudero-Arahuetes, J. L., and López-Díez, J., "Experimental Aerodynamic Characteristics of NACA 0012 Airfoils with Simulated Glaze and Rime Ice," *Journal of Aerospace Engineering (Part G)*, Vol. 215, No. 4, 2001, pp. 229–240.

[10]Huebsch, W. W., and Rothmayer, A. P., "Effects of Surface Ice Roughness on Dynamic Stall," *Journal of Aircraft*, Vol. 39, No. 6, 2002, pp. 945–953.

[11]Politovich, M. K., "Predicting Glaze or Rime Ice Growth on Airfoils," *Journal of Aircraft*, Vol. 37, No. 1, 2000, pp. 117–121.

[12]Wright, W. B., "User Manual for the Improved NASA Lewis Ice Accretion Prediction Code LEWICE 1.6," NASA CR 198355, June 1995.

[13]Van Fossen, G. J., Simoneau, R. J., Olsen, W. A., Jr., and Shaw, R. J., "Heat Transfer Distributions Around Nominal Ice Accretion Shapes Formed on a Cylinder in the NASA Lewis Icing Research Tunnel," AIAA Paper 84-0017, Jan. 1984.

[14]Shin, J., "Characteristics of Surface Roughness Associated with Leading Edge Ice Accretion," AIAA Paper 94-0799, 1994.

[15]Poinsatte, P. E., Van Fossen, G. J., Newton, J. E., and De Witt, K. J., "Heat Transfer Measurements from a NASA 0012 Airfoil," *Journal of Aircraft*, Vol. 28, No. 12, 1991, pp. 892–898.

[16]Poinsatte, P. E., Van Fossen, G. J., Newton, J. E., and De Witt, K. J., "Roughness Effect on Heat Transfer from a NASA 0012 Airfoil," *Journal of Aircraft*, Vol. 28, No. 12, 1991, pp. 908–911.

[17]Pais, M., Singh, S., and Zou, L., "Determination of the Local Heat Transfer Characteristics on Simulated Smooth Glaze Ice Accretions on a NASA 0012 Airfoil," AIAA Paper 88-0292, Jan. 1988.

[18]Dukhan, N., Masiulaniec, K. C., De Witt, K. J., and Van Fossen, G. J., Jr., "Experimental Heat Transfer Coefficients from Ice-Roughened Surfaces for Aircraft Deicing Design," *Journal of Aircraft*, Vol. 36, No. 6, 1999, pp. 948–956.

[19]Dukhan, N., Masiulaniec, K. C., De Witt, K. J., and Van Fossen, G. J., Jr., "Acceleration Effect on the Stanton Number for Castings of Ice-Roughened Surfaces," *Journal of Aircraft*, Vol. 36, No. 5, 1999, pp. 896–898.

[20]Dukhan, N., "Measurements of the Convective Heat Transfer Coefficient from Ice Roughened Surfaces in Parallel and Accelerated Flows," Ph.D. Dissertation, Dept. of Mechanical Industrial and Manufacturing Engineering, Univ. of Toledo, OH, Dec. 1996.

[21]Wood, R. L., and Von Ludwig, D., *Investment Casting for Engineers*, Reinhold, New York, 1952, Chap. 1,3, and 5.

[22]Ruff, G. A., "Quantitative Comparison of Ice Accretion Shapes on Airfoils," *Journal of Aircraft*, Vol. 39, No. 3, 2002, pp. 418–426.

[23]Kline, S. J., and McClintock, F. J., "Describing Uncertainties Analysis in Single Sample Experiment," *Mechanical Engineering Journal*, Vol. 75, No. 1, 1953, pp. 3–8.

[24]Hosni, M. H., Coleman, H. W., and Garner, J. W., "Roughness Shape Effect on Heat Transfer and Skin Friction in Rough-Wall Turbulent Boundary Layer," *International Journal of Heat and Mass Transfer*, Vol. 36, No. 1, 1993, pp. 147–153.

[25]Hosni, M. H., Coleman, H. W., and Taylor, R. P., "Measurement and Calculations of Rough Wall Heat Transfer in the Turbulent Boundary Layer," *International Journal of Heat and Mass Transfer*, Vol. 34, No. 4, 1991, pp. 1067–1082.